Supplementary Material

(Dated: April 13, 2007)

PACS numbers:

I. LOW TEMPERATURE

A. Ground states

The Hamiltonian for the classical Heisenberg magnet on the diamond lattice, with various exchange interactions takes the form

$$\mathcal{H} = \frac{1}{2}\sum_{ij} J_{ij}\mathbf{S}_i \cdot \mathbf{S}_j \ , \tag{1}$$

where i, j denote the sites of the diamond lattice.

One way to find the ground state of the model, is using the well documented Luttinger-Tisza method[1–3]. The method consists of softening the unit length constraint on the $O(3)$ spins $\mathbf{S}_j^2 = 1$, and replacing it with a global constraint

$$\sum_j \mathbf{S}_j^2 = N \ , \tag{2}$$

where N is the number of spins. We then look for the minimum energy configuration of the spin variables, which amounts to finding the minimum eigenvalue of a quadratic form, and putting all the Fourier weight of the spin variables in the minimum eigenvalue mode. If the minimum energy configuration can be realized satisfying the full set of constraints $\mathbf{S}_j^2 = 1$, it must be an exact ground state.

Using an adjacency matrix Γ_{ij} which gives 1 when i, j is a nearest neighbor pair, and 0 otherwise, we can write the exchange interaction in our case as

$$J_{ij} = J_1\Gamma_{ij} + J_2\left((\Gamma^2)_{ij} - 4\delta_{ij}\right) \tag{3}$$

where the combination $\left((\Gamma^2)_{ij} - 4\delta_{ij}\right)$ gives 1 for second neighbors, and 0 otherwise (4 is the number of nearest neighbors in the diamond lattice). This form is possible because for the diamond lattice taking two nearest neighbor steps will either bring you to a 2nd neighbor site, or walk you to a nearest neighbor and back. The n-th power of the adjacency matrix Γ gives in every matrix element the number of n step paths we can make on the lattice network from site i to site j. In this special form, both the J_1 and J_2 terms are diagonalized by the same functions, which are eigenstates of the adjacency matrix.

We now turn to find the eigenvalues of Γ_{ij}. The diamond lattice is an FCC Bravais lattice with a basis of two sites, and therefore in momentum space a quadratic form will have two "bands". The Fourier transform of the adjacency matrix is

$$\Gamma_{\mu\nu}(\mathbf{q}) = 2\begin{pmatrix} 0 & \Lambda(\mathbf{q})e^{+i\theta(\mathbf{q})} \\ \Lambda(\mathbf{q})e^{-i\theta(\mathbf{q})} & 0 \end{pmatrix}_{\mu,\nu} , \tag{4}$$

where the band indices $\mu, \nu = 0, 1$ have been introduced. The non-zero matrix elements are

$$\begin{aligned}\Lambda(\mathbf{q})e^{+i\theta(\mathbf{q})} &= \cos\left(\frac{q_x}{4}\right)\cos\left(\frac{q_y}{4}\right)\cos\left(\frac{q_z}{4}\right) \\ &+ i\sin\left(\frac{q_x}{4}\right)\sin\left(\frac{q_y}{4}\right)\sin\left(\frac{q_z}{4}\right) ,\end{aligned} \tag{5}$$

with $\Lambda(\mathbf{q})$ the magnitude, and $\theta(\mathbf{q})$ the argument of the matrix element. The eigenvalues of Γ_{ij} are then $\pm 2\Lambda(\mathbf{q})$, and we can immediately derive the eigenvalues for J_{ij}

$$\begin{aligned}\epsilon_\pm(\mathbf{q}) &= 4J_2[\Lambda^2(\mathbf{q}) - 1] \pm 2J_1\Lambda(\mathbf{q}) \\ &= 4J_2\left(\Lambda(\mathbf{q}) \pm \frac{J_1}{4J_2}\right)^2 - 4J_2 - \frac{J_1^2}{4J_2} \ .\end{aligned} \tag{6}$$

The minimum eigenvalue is realized in the lower band $\epsilon_-(\mathbf{q})$, and are solutions of an equation of the form $F(\Lambda(\mathbf{q})) = 0$ for some function F. Momenta which satisfy such an equation can generically lie on a surface. The minima occur at a single point ($\mathbf{q} = \mathbf{0}$) for $J_2/J_1 < 1/8$, but on a two-dimensional surface in momentum space for larger J_2/J_1.

The diagonalizing transformation is

$$U_{\mu\nu}(\mathbf{q}) = \frac{1}{\sqrt{2}}\begin{pmatrix} e^{+i\frac{1}{2}\theta(\mathbf{q})} & e^{+i\frac{1}{2}\theta(\mathbf{q})} \\ e^{-i\frac{1}{2}\theta(\mathbf{q})} & -e^{-i\frac{1}{2}\theta(\mathbf{q})} \end{pmatrix}_{\mu,\nu} . \tag{7}$$

The angle $\theta(\mathbf{q})$ determines the relative phase shift between the sublattices.

For $J_2/J_1 < 1/8$ the Luttinger-Tisza method gives the expected Néel phase as the unique ground state (apart from global spin rotations). For larger J_2/J_1 one can construct highly degenerate spiral ground states, each characterized by a single wavevector lying on the "spiral surface" corresponding to the minimum of $\epsilon_-(\mathbf{q})$. Denoting the two FCC sublattices by $\mu = 0, 1$ and the lattice site positions by $\mathbf{r}_j$, the spiral ground states explicitly take the form

$$\mathbf{S}_j^\mu = (-1)^\mu[\hat{\mathbf{x}}\cos\varphi_j^\mu + \hat{\mathbf{y}}\sin\varphi_j^\mu] \tag{8}$$

$$\varphi_j^\mu = \mathbf{q}\cdot\mathbf{r}_j + (-1)^\mu\theta(\mathbf{q})/2, \tag{9}$$

with any wavevector $\mathbf{q}$ on the spiral surface. We have assumed a spiral in the x-y plane, though any two orthonormal unit vectors above will clearly do. (Note that for ferromagnetic $J_1 < 0$, the corresponding ground states are obtained by reversing the spins on one FCC sublattice.)

While this does not exhaust all possible ground states, others occur only at special values of J_2/J_1 or contribute only a finite discrete set. One example of a discrete set of ground states is constructed from wavevectors on the surface differing by half a reciprocal lattice vector. A

particular pair of such momenta with wavevectors of the form $(\pm\pi, q_y, q_z)$ can realize such states over a range of J_2/J_1. As far as order-by-disorder is concerned, one can essentially rule out these additional states on physical grounds. They constitute a finite discrete set and are not smoothly connected to any other ground states, as opposed to the single wavevector "spiral surface" states described above, which can be smoothly distorted into one another. As a result, the latter are sure to have lower free energy due to a larger associated entropy.

We have shown explicitly with the two-wavevector ($(\pm\pi, q_y, q_z)$) state mentioned above, that a bi-quadratic term, $-\sum_{ij} K_{ij}(\mathbf{S}_i \cdot \mathbf{S}_j)^2$ (with all $K_{ij} \geq 0$), expected to capture the effect of fluctuations[4] lowers the energy of the simple one-wavevector spiral ground states relative to this additional discrete set of solutions, when any non-negative nearest neighbor and next-nearest neighbor bi-quadratic interactions are present. This limited analysis agrees with the expectations from our physical arguments, and so it is reasonable to expect that the physical argument applies for the other discrete sets of ground states.

The issue of these other ground states being selected energetically by additional interactions is less clear. For any pairwise interaction we add to the system, the particular pair of momenta $(\pm\pi, q_y, q_z)$ can never do better in energy than a single-wavevector spiral, since the two momenta are related by symmetry, and will therefore have the same energy as a single wavevector spiral with either one of $(\pm\pi, q_y, q_z)$. Addition of an antiferromagnetic J_3 interaction is precisely of this form.

B. Local stability

Henceforth we focus on the regime $J_2/J_1 > 1/8$. Given the massive spiral ground state degeneracy here, the question of stability of long-range order becomes quite delicate. The goal of this subsection is to demonstrate that *entropy* stabilizes long-range order at finite temperature by lifting the degeneracy in the free energy along the spiral surface, *i.e.*, the system undergoes a thermal order-by-disorder transition.

To this end, we start from an arbitrary ground state ordered at momentum $\mathbf{Q}$ with a spin configuration $\overline{\mathbf{S}}_j$ and expand in fluctuations by writing

$$\mathbf{S}_j = \vec{\pi}_j + \overline{\mathbf{S}}_j \sqrt{1 - \vec{\pi}_j^2} \, . \tag{10}$$

The fluctuation field $\vec{\pi}_j$ is constrained such that $\overline{\mathbf{S}}_j \cdot \vec{\pi}_j = 0$ so that the unit-vector constraint remains satisfied. Also, $\vec{\pi}_j$ is restricted to the domain $\vec{\pi}_j^2 \leq 1$. Since the fluctuations are presumed small $\vec{\pi}_j^2 \ll 1$, we shall assume this restriction is always met.

After computing the Jacobian for the variable transformation, the partition function becomes

$$\begin{aligned} \mathcal{Z} &= \int \mathcal{D}\mathbf{S} e^{-\beta H} \prod_{\mathbf{r}} \delta[\mathbf{S}_j^2 - 1] \\ &= \int \mathcal{D}\vec{\pi} e^{-\beta H} \prod_{\mathbf{r}} \left[1 - \vec{\pi}_j^2\right]^{-1/2} \, . \end{aligned} \tag{11}$$

An expansion in small fluctuations can be controlled at low temperatures. Assuming the spins $\overline{\mathbf{S}}_j$ lie in the x-y plane, we parametrize the fluctuations as follows,

$$\vec{\pi}_j = \hat{\mathbf{z}}\phi_j + [\hat{\mathbf{z}} \times \overline{\mathbf{S}}_j]\chi_j \, , \tag{12}$$

thereby automatically satisfying the constraint $\overline{\mathbf{S}}_j \cdot \vec{\pi}_j = 0$. The partition function can now be expressed in terms of an action,

$$\mathcal{Z} = \int \mathcal{D}\phi \mathcal{D}\chi e^{-\mathcal{S}} \, , \tag{13}$$

with all the variables χ_j, ϕ_j being integrated over the entire range of real numbers. Retaining the leading corrections to the Gaussian theory, the action can be written as $\mathcal{S} = \mathcal{S}_2 + \mathcal{S}_3 + \mathcal{S}_4$, where

$$\begin{aligned} \mathcal{S}_2 &= \frac{\beta}{2} \sum_{ij} \left[\tilde{J}_{ij}\phi_i\phi_j + W_{ij}\chi_i\chi_j \right] - \frac{1}{2}\sum_j [\phi_j^2 + \chi_j^2] \\ \mathcal{S}_3 &= \frac{\beta}{2} \sum_{ij} K_{ij}\phi_i \left(\phi_j^2 + \chi_j^2\right) \\ \mathcal{S}_4 &= \frac{\beta}{8} \sum_{ij} W_{ij} \left(\phi_i^2 + \chi_i^2\right)\left(\phi_j^2 + \chi_j^2\right) \, . \end{aligned} \tag{14}$$

Here $\tilde{J}_{ij}$ is simply the exchange matrix J_{ij} shifted by a constant, such that all the eigenvalues are non-negative and the ground state space corresponds to the kernel of this matrix. We have also defined the matrices $W_{ij} = \tilde{J}_{ij}\left(\overline{\mathbf{S}}_j \cdot \overline{\mathbf{S}}_i\right)$ and $K_{ij} = \tilde{J}_{ij}\left[\hat{z} \cdot \left(\overline{\mathbf{S}}_j \times \overline{\mathbf{S}}_i\right)\right]$. The Jacobian factor has been absorbed into the action, giving rise to the last summation in $\mathcal{S}_2$.

According to Eq. (12), fluctuations out of the spiral plane are described by ϕ_j, while χ_j describes in-plane fluctuations. Long-range order will occur if these fluctuations can always be made small by going to sufficiently low temperature. The χ_j fluctuation modes (the eigenvalues of the matrix W_{ij}) are

$$\begin{aligned} &\Omega_{0,1}(\mathbf{q}) = 2J_2\left[-2 + \Lambda(\mathbf{q}-\mathbf{Q})^2 + \Lambda(\mathbf{q}+\mathbf{Q})^2\right] - \epsilon_-^{\min} \\ &\mp J_1\Big[\Lambda(\mathbf{q}-\mathbf{Q})^2 + 2B\Lambda(\mathbf{q}+\mathbf{Q})\Lambda(\mathbf{q}-\mathbf{Q}) + \Lambda(\mathbf{q}+\mathbf{Q})^2\Big]^{1/2} \, , \end{aligned} \tag{15}$$

where $\epsilon_-^{\min}$ corresponds to the minimum value of $\epsilon_-(\mathbf{q})$, and $B = \cos(\theta(\mathbf{q}-\mathbf{Q}) + 2\theta(\mathbf{Q}) - \theta(\mathbf{q}+\mathbf{Q}))$. The χ_j fluctuation modes have only a single gapless mode, corresponding to the symmetry-required Goldstone mode at zero momentum $\mathbf{q} = 0$. Consequently, fluctuations in

χ_j are clearly well-behaved at low temperature. Subtleties with long-range order arise from the ϕ_j fluctuations, which connect the degenerate ground states. At the Gaussian level and to leading order in temperature, the ϕ_j propagator is

$$G^0_{ij} = \langle \phi_j \phi_i \rangle_0 = \tilde{J}^{-1}_{ij}. \tag{16}$$

In momentum space, the associated normal mode frequencies $\kappa_0(\mathbf{q})$ and $\kappa_1(\mathbf{q})$ are defined by

$$\kappa_{0,1}(\mathbf{q}) \equiv \epsilon_{\mp}(\mathbf{q}) - \epsilon_{-}^{\min} \ . \tag{17}$$

It follows that the fluctuation amplitude for ϕ_j naively *diverges*,

$$\langle \phi_j^2 \rangle_0 \sim T \int_{\mathbf{q}} \frac{1}{\kappa_0(\mathbf{q})} \to \infty \ , \tag{18}$$

since $\kappa_0(\mathbf{q})$ vanishes for any $\mathbf{q}$ on the spiral surface due to the continuous ground state degeneracy.

Higher-order corrections in temperature, however, lift the surface degeneracy, thus curing the above divergence and stabilizing long-range order. Perturbation theory in temperature suffers similar divergences as found above, and hence we employ a self-consistent treatment to obtain corrections to the ϕ_j fluctuations. The ϕ_j propagator obtained from the full action $\mathcal{S}$ defined above is

$$G_{ij} = \langle \phi_j \phi_i \rangle = \left[\tilde{J}_{ij} + \tilde{\Sigma}_{ij} \right]^{-1}, \tag{19}$$

where $\tilde{\Sigma}_{ij}$ is the *self-energy*. In particular, we are interested in the self-energy correction to $\kappa_0(\mathbf{p})$, which we will denote $\tilde{\Sigma}(\mathbf{p})$, for momenta $\mathbf{p}$ along the spiral surface. Other components of the self energy are not required to cure the divergence, and so we can safely neglect them as a first approximation.

To proceed, we first assume that thermal fluctuations indeed break the surface degeneracy, and then find the leading corrections self-consistently. In momentum space, the result of a 1-loop self-consistent diagrammatic calculation is the equation

$$\Sigma_{\mu\nu}(\mathbf{k}) = T \int_{\mathbf{q}} G_{\mu\nu}(\mathbf{q}) \Big[W_{\mu\nu}(\mathbf{k}-\mathbf{q}) + \sum_{\lambda\rho} K_{\mu\lambda}(\mathbf{k}-\mathbf{q}) W^{-1}_{\lambda\rho}(\mathbf{k}-\mathbf{q}) K_{\rho\nu}(\mathbf{k}-\mathbf{q}) \Big] - T\delta_{\mu,\nu} \ , \tag{20}$$

with $G_{\mu\nu}(\mathbf{q})$, $K_{\mu\nu}(\mathbf{q})$, and $W_{\mu\nu}(\mathbf{q})$ the Fourier transform of the matrices G_{ij}, K_{ij} and W_{ij} respectively. The self energy correction to $\kappa_0(\mathbf{p})$ is obtained by taking

$$\tilde{\Sigma}(\mathbf{k}) = \frac{1}{2} \left(\Sigma_{11}(\mathbf{k}) - e^{-i\theta(\mathbf{k})} \Sigma_{12}(\mathbf{k}) - e^{+i\theta(\mathbf{k})} \Sigma_{21}(\mathbf{k}) + \Sigma_{22}(\mathbf{k}) \right) . \tag{21}$$

Next, we assume that $\tilde{\Sigma}(\mathbf{p}) \sim T^{\alpha} \Sigma(\mathbf{p})$, where $\alpha < 1$, $\Sigma(\mathbf{p})$ is temperature-independent, and $\Sigma(\pm\mathbf{Q}) = 0$; the last condition simply asserts that the symmetry-required Goldstone modes at the ordering wavevectors are preserved. With these assumptions, we obtain a self-consistent equation of the form

$$\tilde{\Sigma}(\mathbf{k}) = T \int_{\mathbf{q}} V(\mathbf{q}, \mathbf{k}) G(\mathbf{q}) \ , \tag{22}$$

with $G(\mathbf{q}) = \left[\kappa_0(\mathbf{q}) + \tilde{\Sigma}(\mathbf{q}) \right]^{-1}$. The integrand $V(\mathbf{q}, \mathbf{k})$ takes on the form

$$V(\mathbf{q}, \mathbf{k}) = \frac{2}{\Omega_0(\mathbf{k}-\mathbf{q}) \Omega_1(\mathbf{k}-\mathbf{q})} \Big[(A+1) \kappa_0(\mathbf{k}-\mathbf{q}-\mathbf{Q}) \kappa_0(\mathbf{k}-\mathbf{q}+\mathbf{Q}) \kappa_1(\mathbf{k}-\mathbf{q}-\mathbf{Q}) + (1-A) \kappa_0(\mathbf{k}-\mathbf{q}-\mathbf{Q}) \kappa_1(\mathbf{k}-\mathbf{q}-\mathbf{Q}) \kappa_1(\mathbf{k}-\mathbf{q}+\mathbf{Q}) + (\mathbf{Q} \to -\mathbf{Q}) \Big] \ , \tag{23}$$

where $A = \cos(\theta(\mathbf{k}) - \theta(\mathbf{q}) + \theta(\mathbf{Q}) - \theta(\mathbf{k}-\mathbf{q}+\mathbf{Q}))$.

At low-temperatures, the integral in Eq. 22 is dominated by momenta near the spiral surface due to the propagator $G(\mathbf{q})$. By contrast, the function $V(\mathbf{q}, \mathbf{k})$ is well behaved and does not lead to any additional singular behavior. Hence it is sufficient to replace $V(\mathbf{q}, \mathbf{k}) \to V(\mathbf{q}_s, \mathbf{k})$ under the integral, where $\mathbf{q}_s$ lies precisely on the surface in the direction of $\mathbf{q}$. One can show that $V(\mathbf{q}_s, \pm\mathbf{Q}) = 0$, so that the Goldstone modes are indeed preserved within our self-consistent treatment. Furthermore, one can approximate $G(\mathbf{q}) \approx \left[v^2 (q - q_s)^2 + T^{\alpha} \Sigma(\mathbf{q}) \right]^{-1}$ in the integrand. The temperature dependence can then be scaled out of the integral, implying a power $\alpha = 2/3$ consistent with our assumptions.

The divergent fluctuations are thus cured by the onset of a thermally induced splitting $\Delta \sim T^{2/3}$ along the spiral surface. Consequently, ordering at finite temperature will occur, despite the massive ground state degeneracy.

C. Global selection

In the previous subsection we found that thermal fluctuations stabilize long-range order at finite temperature. Here we address the more specific (and simpler) question of which state among the degenerate set is favored. At finite temperature, entropy selects the states minimizing the free energy $F = E - TS$ (E is energy, S entropy), which usually are those with the highest density of nearby low-energy states. Let us start from an arbitrary spiral with ordering wavevector $\mathbf{Q}$, and expand in fluctuations as outlined in the previous subsection. At low temperatures, for our purpose here it suffices to retain only the first two terms in the Gaussian action S_2. Integrating over the fluctuation fields, we then obtain the leading T-

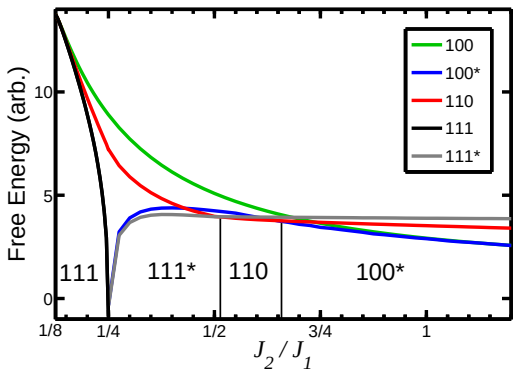

FIG. 1: Free energy versus J_2/J_1 along high-symmetry directions in the Brillouin zone.

and $\mathbf{Q}$-dependent contribution to the free energy,

$$F(\mathbf{Q}) = -T\ln(\mathcal{Z}) \sim T\left(Tr\left[\ln(\tilde{J}/2\pi T)\right] + Tr\left[\ln(W(\mathbf{Q})/2\pi T)\right]\right), \tag{24}$$

where $\hat{J}, \hat{W}$ denote the matrices defined in the previous subsection and we have explicitly labeled the $\mathbf{Q}$-dependence in $\hat{W}$. The first term is $\mathbf{Q}$-independent and thus does not distinguish the states on the spiral surface. This is accomplished, however, by the second term, which can be easily computed numerically as a function of $\mathbf{Q}$ to obtain the global free energy minima. The resultant free-energy splittings are illustrated through the coloring of the surfaces in Fig. 2 of main text. Also, we display in Fig. 1 the free energy along high-symmetry directions as a function of J_2/J_1. Here, 111* refers to six momenta located along the "holes" which develop in the surface for $J_2/J_1 > 1/4$, and 100* corresponds to four momenta located around the 100 directions (see main text).

D. Specific heat

The anomalous low temperature dependence of the free energy will manifest itself in thermodynamic quantities. In this section we show explicitly how the specific heat varies with temperature in this regime.

The heat capacity $C_v = -T\left(\frac{\partial^2 F}{\partial T^2}\right)_{V,N}$ can be found from our low temperature expression for the free energy. Including only the anomalous part of the self energy, while neglecting all analytic corrections higher order in T, we modify (24) to

$$\begin{aligned} F \sim & T\left(Tr\left[\ln[(\tilde{J}+\tilde{\Sigma})/2\pi T]\right] + Tr\left[\ln(W(\mathbf{Q})/2\pi T)\right]\right) \\ \sim & -A_1 T\ln(T) + A_2 T + T\int_{\mathbf{q}} \ln[(\kappa_0(\mathbf{q}) + T^{2/3}\Sigma(\mathbf{q}))]\,. \end{aligned} \tag{25}$$

To find the behavior of the integral at low temperatures, it is useful to consider

$$\frac{\partial(F/T)}{\partial T} \sim -\frac{A_1}{T} + \frac{2}{3}T^{-1/3}\int_{\mathbf{q}} \frac{\Sigma(\mathbf{q})}{(\kappa_0(\mathbf{q}) + T^{2/3}\Sigma(\mathbf{q}))]} \tag{26}$$

scaling temperature out of the momentum integral on the right hand side. In the same manner we proceeded for the integral in (22), we find $\int_{\mathbf{q}} \frac{\Sigma(\mathbf{q})}{(\kappa_0(\mathbf{q})+T^{2/3}\Sigma(\mathbf{q}))]} \sim T^{-1/3}$ so that $\frac{\partial(F/T)}{\partial T} \sim -\frac{A_1}{T} + \frac{2}{3}T^{-2/3}B$. The low temperature form of the free energy is

$$F \sim -A_1 T\ln(T) + A_2 T + A_3 T^{4/3} \tag{27}$$

where $A_{1,2,3}$ are constants. From this form it follows that the heat capacity is

$$C_v^{\text{classical}}(T) = A + BT^{1/3}\,. \tag{28}$$

E. Spin Waves

The fluctuation stiffness modes discussed above are different but related to the classical spin-wave modes in this model. The spin waves are obtained by considering the classical equations of motion

$$\partial_t \mathbf{S}_j = \left[\sum_i J_{ij}\mathbf{S}_i\right] \times \mathbf{S}_j\,. \tag{29}$$

Using the parametrization from Eqs. (10),(12) for weak fluctuations, we find

$$\begin{aligned} \partial_t \phi_j &= -\sum_i W_{ij}\chi_i \\ \partial_t \chi_j &= +\sum_i J_{ij}\phi_i\,. \end{aligned} \tag{30}$$

The normal mode frequencies are then the square roots of the eigenvalues of the matrix $\hat{A} = \hat{W}\cdot\hat{J}$.

For momenta near the spiral surface, we find the approximate form of the lower branch of these eigenvalues

$$\begin{aligned} &\omega_0(\mathbf{q})^2 \approx \kappa_0(\mathbf{q})\Omega_0(\mathbf{q})\Omega_1(\mathbf{q}) \\ &/\Big[[1+\cos(\gamma_1)]\,\kappa_0(\mathbf{q}-\mathbf{Q}) + [1+\cos(\gamma_2)]\,\kappa_0(\mathbf{q}+\mathbf{Q}) \\ &+ [1-\cos(\gamma_1)]\,\kappa_1(\mathbf{q}-\mathbf{Q}) + [1-\cos(\gamma_2)]\,\kappa_1(\mathbf{q}+\mathbf{Q})\Big]\,, \end{aligned} \tag{31}$$

with $\gamma_1 = \theta(\mathbf{q}) - \theta(\mathbf{Q}) - \theta(\mathbf{q}-\mathbf{Q})$ and $\gamma_2 = \theta(\mathbf{q}) + \theta(\mathbf{Q}) - \theta(\mathbf{q}+\mathbf{Q})$. The denominator never vanishes when $\mathbf{q}$ is near the spiral surface, since all the terms are semipositive definite, and in general all of them vanish only when $\mathbf{q} = 0$ which is far away from the spiral surface, unless $J_2/J_1 \approx 1/8$. For $\mathbf{q}$ near the surface point $\mathbf{q}_s$, we find the frequency vanishes as $\omega_0(\mathbf{q})^2 \approx (q-q_s)^2\, v(\mathbf{q}_s,\mathbf{Q})^2$ with $v(\mathbf{q}_s,\mathbf{Q})$ having dimensions of velocity.

II. HIGH TEMPERATURE

This section is concerned with analytically describing the spin correlations at temperatures above T_c. Remarkably, these allow one to probe directly the underlying ground state surface in the "spiral spin liquid" regime occurring over a broad temperature range. In the disordered phase above T_c, the spins fluctuate strongly, and it is reasonable that the unit length constraint on the individual spins can be relaxed. Hence we employ the "spherical" approximation, replacing the local unit-vector spin constraint with the global constraint $\sum_j \mathbf{S}_j^2 = N$, N being the total number of sites. The spin correlations determined via Monte Carlo numerics are described *quantitatively* within this scheme, except very near T_c where entropic effects are dramatic.

The partition function for this model is

$$\mathcal{Z} = \int \mathcal{D}\mathbf{S} d\lambda e^{-\beta H - i\lambda(\sum_j \mathbf{S}_j^2 - N)} \ , \tag{32}$$

where λ is a Lagrange multiplier enforcing the global constraint. To proceed we employ a saddle-point approximation, replacing $i\lambda \to \beta\Delta(T)/2$, where $\Delta(T)$ is the saddle-point value to be determined. The spin correlation function is then

$$\langle \mathbf{S}_i \mathbf{S}_j \rangle = 3T \left[J_{ij} + \delta_{ij}\Delta(T) \right]^{-1} \ . \tag{33}$$

Upon integrating over the spins, one obtains the saddle point equation for $\Delta(T)$:

$$\frac{1}{T} = \frac{3}{2} \int_{\mathbf{q}} \sum_{j=0,1} \frac{1}{\kappa_j(\mathbf{q}) + \Delta(T)} \ . \tag{34}$$

Equations (33) and (34) together determine the spherical model spin correlations. In particular, the momentum-space correlation function for spins on the same FCC sublattice is given by

$$S^{AA}(\mathbf{q}) \sim T \left[\frac{1}{\kappa_0(\mathbf{q}) + \Delta(T)} + \frac{1}{\kappa_1(\mathbf{q}) + \Delta(T)} \right], \tag{35}$$

while the correlation between spins on opposite FCC sublattices is

$$S^{AB}(\mathbf{q}) \sim T e^{-i\theta(\mathbf{q})} \left[\frac{-1}{\kappa_0(\mathbf{q}) + \Delta(T)} + \frac{1}{\kappa_1(\mathbf{q}) + \Delta(T)} \right]. \tag{36}$$

The full structure factor, as measured in experiment, is

$$S(\mathbf{q}) = S^{AA}(\mathbf{q}) + \mathrm{Re}[S^{AB}(\mathbf{q})]. \tag{37}$$

Notice that the spin correlation $S^{AA}(\mathbf{q})$ depends on momentum only through the function $\Lambda(\mathbf{q})$. ($\mathbf{S}^{AB}(\mathbf{q})$ has additional momentum dependence through $\theta(\mathbf{q})$.) Hence it is highly desirable to isolate this contribution, as $S^{AA}(\mathbf{q})$ collapses onto a known one-dimensional curve when plotted versus $\Lambda(\mathbf{q})$. We have extracted $S^{AA}(\mathbf{q})$ in our Monte Carlo simulations for $J_2/J_1 = 0.2, 0.25, 0.4, 0.6, 0.85$, and indeed find that in all cases for $T > T_c$ the correlation function data collapse well when plotted versus $\Lambda(\mathbf{q})$. Furthermore, in all these cases one finds *quantitative* agreement with the analytic result Eq. (35), with only a single fitting parameter corresponding to an overall scaling. The excellent agreement obtained here is illustrated in the main text for $J_2/J_1 = 0.85$. The peaks in these figures correspond to values of $\Lambda(\mathbf{q})$ defining the spiral surface, thus implying that spin configurations near the surface dominate the physics. This is the spiral spin liquid regime.

Naively, isolating $S^{AA}(\mathbf{q})$ experimentally appears more difficult. Fortunately, one can extract this component from the full structure factor by noting that for reciprocal lattice vectors $\mathbf{K} = 4\pi(1,0,0)$ we have

$$S^{AA}(\mathbf{q}) = \frac{1}{2}[S(\mathbf{q}) + S(\mathbf{q}+\mathbf{K})] \ , \tag{38}$$

which follows from the definition of the Fourier transform. It would be extremely interesting to perform a similar analysis on experimental neutron scattering data, which would require single crystals. The spiral surface could then be extracted quite simply as follows. Display momenta in the first Brillouin zone corresponding to the highest intensity points within some threshold—the surface is mapped out when an appropriate threshold is chosen. Such an analysis was carried out for the Monte Carlo structure factor, the result of which are shown in the main text.

Obtaining single crystal samples is often challenging, so it is highly desirable (and of current experimental relevance) to have a way of detecting the spiral surface in neutron data for powder samples. The full structure factor can be numerically "powder-averaged" by performing an angular integration for a given wavevector magnitude Q:

$$S_{\mathrm{ave}}(Q) = \int \sin\theta d\theta d\varphi S(\mathbf{Q}), \tag{39}$$

where θ and φ are polar and azimuthal angles specifying the direction of $\mathbf{Q}$. The spiral surface is then indirectly revealed as a peak in $S_{\mathrm{ave}}(Q)$ over the range of Q for which the surface occurs. Existing neutron data for $MnSc_2S_4$ powder samples indeed reveal a broad peak in the structure factor in agreement with our predictions for the spiral spin liquid regime. Furthermore, excellent agreement with powder neutron data for $CoAl_2O_4$ can be obtained by assuming that $J_2/J_1 \approx 1/8$ for this material. Fig. 2 displays the predicted powder-averaged structure factor, which exhibits peaks and valleys that correspond well to those observed experimentally[5]. The low-T_c in this vicinity of J_2/J_1 is further consistent with the large frustration parameter observed for $CoAl_2O_4$.

III. MONTE CARLO SIMULATIONS

In our numerical simulations of the parent Hamiltonian we used classical Monte Carlo techniques employing

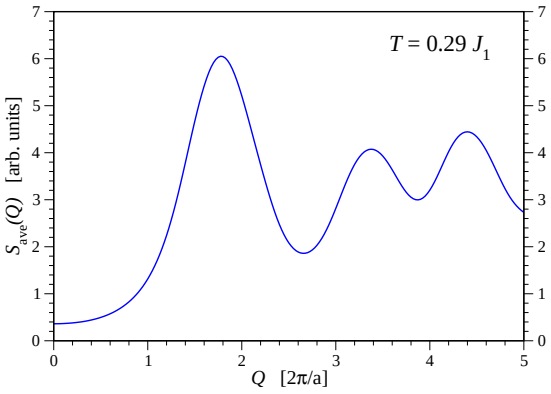

FIG. 2: Powder-averaged structure factor in the spherical model with $J_2/J_1 \approx 1/8$. The data reproduce well the diffuse scattering observed in powder neutron experiments.

a parallel tempering scheme[6] where multiple replicas of the system are simulated simultaneously over a range of temperature. Thermal equilibration at the ordering transition can be dramatically increased by swapping replicas between neighboring temperature points. For each ratio of competing interactions J_2/J_1 the simulated temperature set has been chosen such that thermal equilibration in the parallel tempering scheme is maximized which can be achieved by accumulating temperature points in the vicinity of the phase transition applying a recently introduced feedback technique[7,8]. A distinct double-peak structure in energy histograms measured at the ordering temperature, shown in Fig. 3, indicate a strong first-order transition. The implementation of these algorithms was based on the ALPS libraries[9].

[1] Lyons, D. H., Kaplan, T. A., Dwight, K. & Menyuk, N. Classical theory of the ground spin-state in cubic spinels. *Phys. Rev.* **126**, 540–555 (1962).

[2] Luttinger, J. M. & Tisza, L. Theory of dipole interaction in crystals. *Phys. Rev.* **70**, 954–964 (1946).

[3] Luttinger, J. M. A note on the ground state in antiferromagnetics. *Phys. Rev.* **81**, 1015–1018 (1951).

[4] Henley, C. L. Ordering by disorder: Ground-state selection in fcc vector antiferromagnets. *Journal of Applied Physics* **61**, 3962–3964 (1987).

[5] Krimmel, A., Tsurkan, V., Sheptyakov, D. & Loidl, A. Spin liquid versus spin solid in A-site spinels. *Physica B* **378-380**, 583–584 (2006).

[6] Hukushima, K. & Nemoto, K. Exchange Monte Carlo method and application to spin glass simulations. *J. Phys. Soc. Jpn.* **65**, 1604–1608 (1996).

[7] Trebst, S., Huse, D. A. & Troyer, M. Optimizing the ensemble for equilibration in broad-histogram Monte Carlo simulations. *Phys. Rev. E* **70**, 046701 (2004).

[8] Katzgraber, H. G., Trebst, S., Huse, D. A. & Troyer, M. Feedback-optimized parallel tempering Monte Carlo. *J. Stat. Mech.* **2006**, P03018 (2006).

[9] Alet, F. *et al.* The ALPS project: open source software for strongly correlated systems. *J. Phys. Soc. Jpn. Suppl.* **74**, 30–35 (2005).

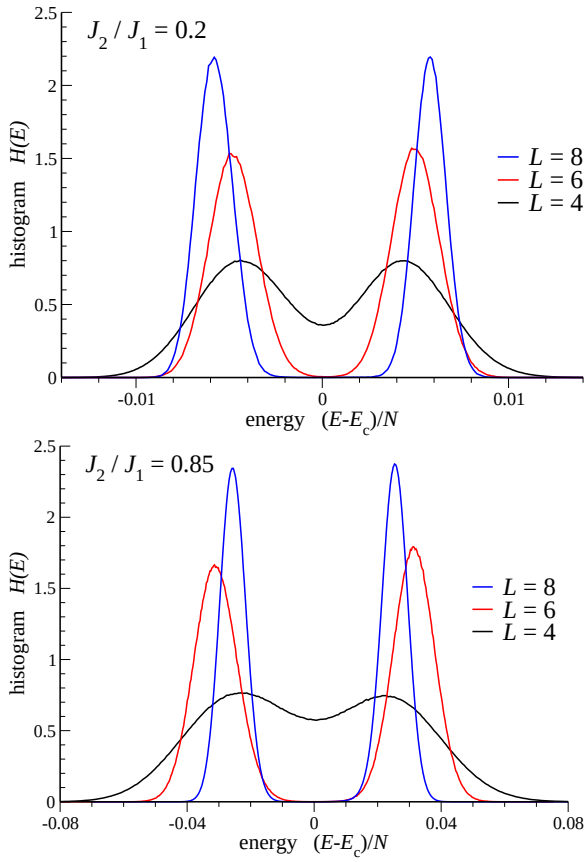

FIG. 3: Energy histograms at the ordering temperature T_c for various system sizes. The distinct double-peak structure indicates a strong first-order transition.